A decentralized biomass torrefaction reactor concept. Part I: Multi-scale analysis and initial experimental validation

A Decentralized Biomass Torrefaction Reactor Concept. Part I: Multi-Scale Analysis and Initial Experimental Validation

Kevin S. Kung[1,2,3], Santosh Shanbhogue[1,2], Alexander H. Slocum[1,2], and Ahmed F. Ghoniem[1,2]

[1] *Department of Mechanical Engineering, MIT, Cambridge, MA*

[2] *Tata Center for Technology and Design, MIT, Cambridge, MA*

[3] *Department of Biological Engineering, MIT, Cambridge, MA*

ABSTRACT:

A new, simplified biomass torrefaction reactor concept that operates under oxygen-lean conditions is proposed as a potential way to downscale torrefaction reactors for small- and medium-scale applications. To verify the feasibility of the concept, a multi-scale analysis was conducted to understand the design requirements, underlying chemistry, intra-particle effects, and overall reactor-scale heat transfer. We demonstrate that the heat transfer within the reactor and the appropriate reactor height is largely determined by gas-phase advection. Finally, by implementing a laboratory-scale reactor and operating it under diverse conditions, we show that such a design can indeed satisfy the requirements for torrefaction. This lays the basis for the second part of this two-part paper, where we develop a detailed mathematical model for this concept. In future studies, we will also systematically define and map the performance metrics and reaction conditions in order to understand the scaling laws for potential commercialization of this concept.

Highlights

- A small to medium scale, decentralized biomass torrefaction reactor operating authothermally was proposed.
- Multi-scale analysis incorporating reaction thermochemistry and reactor heat transfer was conducted.
- An experimental set-up encapsulating this reactor concept was proposed and implemented.
- The experimental measurements on the temperature and solid outputs demonstrate initial data consistent with torrefaction.
- Detailed mathematical modeling and systematic quantification of the reactor performance are the next steps.

Keywords: Biomass; torrefaction; reactor design; multi-scale modeling.

Corresponding Author: Kevin S. Kung

Address: Room 3-339, 77 Massachusetts Avenue, Cambridge, MA 02139

Email: kkung@mit.edu

Telephone: +1.617.324.4449

1. Introduction

Most biomass residues, in their raw form, are not useful or desirable: they can be wet, loose, and bulky. This makes them difficult and expensive to collect, transport, process, and utilize in energy applications. Furthermore, specific biomass types such as agricultural wastes are seasonal, making it a challenge to store for long-term consumption during the

off-seasons. In order to address these challenges, many studies have considered biomass torrefaction, which is a thermochemical process whereby biomass is heated to a temperature of around 200-320°C. Under such conditions, it releases low-energy volatile molecules and densifies into a carbon-rich, energy-dense solid called torrefied biomass, with improved characteristics. For example, torrefied biomass is mostly hydrophobic, making it resistant to moisture attack and extending its shelf life [1]. Torrefied biomass also has improved energy density, which effectively lowers its transportation cost [2]. Finally, it takes less energy to grind torrefied biomass into smaller pieces than it does to grind raw biomass. For many thermal applications where the input fuel must first be pulverized, this saves on the pre-processing costs [3].

To date, various torrefaction reactors have been developed on a laboratory or commercial scale. These have been described elsewhere [4-6]. Table S1 in the supplementary section summarizes some of these reactors as well as their intended production capacity. Most of the torrefaction reactors developed or proposed to date have considerable production capacities, typically on the order of 10^4-10^5 kg day^{-1}. While these installations may be effectively used when co-located with large, centralized biomass waste generation sources (such as a lumber mill or an agricultural processing mill), their current designed scale is incompatible for deployment in rural and decentralized areas, where much of the biomass waste is actually being produced.

In order to understand the scale requirements of decentralized biomass torrefaction, let us consider a potential use case in India using rural agricultural residues. While there is a

wide distribution in the sizes, the typical farm size in South Asia is around 1.3×10^4 m^2 (1.3 hectares) [7]. While the yield of agricultural residues per hectare is highly dependent upon various factors, we assume that a representative value is 0.225 kg m^{-2} on harvest [8]. Thus, a representative farm in rural India may have about 3,000 kg of post-agricultural residues to be processed, and these farms are spread geographically amongst a large rural region. For a portable, low-cost, low-maintenance torrefaction reactor that can move from farm to farm on a daily basis, it must have a biomass processing capacity of on the order of 10^3 kg day^{-1} [9]. This represents the need to downscale current torrefaction reactor designs by a factor of at least 10.

Svanberg *et al.* [10], in characterizing the capital cost of current torrefaction reactor designs, noted that almost all existing designs enforce a near-inert condition inside the biomass reactor, and this is one main reason why the capital cost and operational complexity has remained prohibitively high in small- to medium-scale torrefaction applications. That study further commented that if this inert requirement can be relaxed, then both the capital and operational costs associated with the reactor operation are likely to be reduced. In the search of a simplified torrefaction reactor design for decentralized deployment, this low-oxygen torrefaction appears to be an attractive option for further experimentation.

It is only in recent years, that torrefaction in an oxygen-lean environment has been the subject of laboratory studies. Some studies [11] have found negligible effect of the presence of oxygen on the overall yield and efficiency, while others [12-14] have found that under

highly oxidative environments, there are sacrifices in output characteristics. None of these studies, to the best of our knowledge, have moved beyond an idealized batch-type furnace towards a more realistic reactor design, and it is currently unknown how these effects play out on a continuous reactor prototype.

This two-part paper has been written with the above-mentioned goal in mind, of designing a biomass torrefaction reactor for small- to medium-scale operations in rural, decentralized regions, and validating its functionality. In Part I, we describe the concept and analysis of an oxygen-lean torrefaction reactor concept that greatly simplifies the reactor design. We then built and tested a laboratory-scale prototype to demonstrate that our concept does indeed meet the requirements for biomass torrefaction. In Part II, we will develop a more detailed and versatile mathematical model that fits with our experimental observations, in order to better understand the design and scaling laws of this reactor concept.

2. Basis and Derivation of an Oxygen-Lean Torrefaction Reactor Concept

We begin with a simple moving bed, counterflow continuous reactor design, inspired by similar designs in biomass gasifiers. A schematic of the design is shown in Figure 1.

In this design, raw biomass is continuously fed from the top into a moving bed. At the bottom, a turning auger continuously removes the torrefied biomass from the moving bed, allowing the incoming biomass column to migrate downwards by gravity. Air (at room temperature) is introduced near the bottom of the reactor. With an initial heat source to

start the reaction, we hypothesize that the incoming air will continuously combust with a limited amount of biomass in the reaction zone at a reaction temperature that is at or above the auto-ignition point of the specific type of biomass. We further hypothesize that by varying the amount of air injecting at this location, we can increase or decrease the extent of biomass combustion, thereby regulating the steady-state temperature profile in this reaction zone. As the incoming air is consumed by the combustion, this results in a low-oxygen environment that supports torrefaction at the bottom of the moving bed. As the reacting air, volatiles, and flue gas mixture travels upwards through the moving bed in a counter-flow manner, it cools and is exhausted from the top of the reactor. Therefore, while the biomass is traveling downwards, it is also being heated until it reaches torrefaction temperature at the bottom of the moving bed. To the side of the moving bed, there is an extension with a length of the auger conveying biomass away from the moving bed. This length serves two functions. Firstly, as the biomass at the bottom of the moving bed is hot, it needs to be cooled before emerging from the reactor, or else there may be a spontaneous combustion. Therefore, the primary function of the auger extension is to cool the hot, torrefied biomass. Therefore, this section is also referred to as the “char-cooling segment”. Secondly, the auger flights and the inner diameter of the char-cooling segment form quite a tight seal, such that it prevents most of the injected air, volatiles, and post-combustion flue gas mixture from escaping sideways with the cooling char, but rather directs almost all of it upwards through the moving bed. In order for this to happen, the pressure drop for the gas across the char-cooling segment should be higher than that for the gas across the moving bed. This means that for the preliminary design, the char-cooling segment should be at least longer than the height of the moving bed.

3. Multiscale Analysis of the Reactor Concept

It is prudent to carry out an initial analysis of our proposed reactor concept, in order to verify that it actually meets the various chemistry and heat transfer requirements for torrefaction. We need to consider processes at different scales: at a molecular scale, chemical kinetics of solid devolatilization dictates the temperature and timescale requirements for the torrefaction reaction. At the particle scale, thermal thickness in the biomass particles may affect the homogeneity of the output. Finally, at the reactor scale, the heat transfer mechanisms need to be reconciled with the temperature and timescale requirements identified earlier. A more detailed mathematical model of the reactor is beyond the scope of the present paper, but will be presented in a subsequent study to fit the experimental data obtained in the present paper.

3.1 Micro-Scale Kinetics and Thermochemistry

In order to describe the solid devolatilization process, we utilized an existing kinetic model proposed by Bates and Ghoniem [15], developed for the case of willow (Figure 2). In this model, the solid-phase devolatilization following a two-step lump-sum process. First, the raw biomass (A) can either decompose into volatile gas (V1) or become solid intermediate (B). Then, the solid intermediate (B) becomes either volatile gas (V2) or char (C). Each of these reactions are assumed to be first-order Arrhenius in nature. In addition, for the drying of biomass, we utilized a simplified model proposed by Peters and Bruch [16], where water bound to the biomass (M(b)) in the solid phase becomes unbound (M(ub))in the gas phase as a first-order Arrhenius-type process.

This gives us the following rate equations:

$$A_{(s)} \rightarrow B_{(s)}, k_1 = 2.48 \times 10^4 \exp\left(\frac{-75976}{RT}\right),$$

$$A_{(s)} \rightarrow V_{1(g)}, k_{\mathrm{V1}} = 3.23 \times 10^7 \exp\left(\frac{-114214}{RT}\right),$$

$$B_{(s)} \rightarrow C_{(s)}, k_2 = 1.10 \times 10^{10} \exp\left(\frac{-151711}{RT}\right),$$

$$B_{(s)} \rightarrow V_{2(g)}, k_{\mathrm{V2}} = 1.59 \times 10^{10} \exp\left(\frac{-151711}{RT}\right),$$

$$M_{(\mathrm{b})} \rightarrow M_{(\mathrm{ub})}, k_{\mathrm{M}} = 5.56 \times 10^6 \exp\left(\frac{-87900}{RT}\right).$$

In order to understand the timescales ($\sim k_i^{-1}$) necessary to undertaken each of these *i*th reactions, in Figure 3(a) we plot these various timescales as a function of temperature. As we can see, for the 200-300°C range, which is typical for torrefaction, the characteristic timescale τ_{res} for solid devolatilization ranges from 10 minutes to 10 days. Moreover, drying (dashed purple line) is comparatively fast, ranging from 10 seconds to 10 minutes. Therefore, the solid residence time inside the reactor is imposed by the solid devolatilization kinetics. To understand what this means for the reactor dimensions, we utilize the desired reactor throughput of $\dot{m}_{\mathrm{BM}}$ =5,000 kg day^{-1} as derived previously. The reactor volume V_r necessary to process $\dot{m}_{\mathrm{BM}}$ of biomass is given by $V_r \sim \dot{m}_{\mathrm{BM}} \tau_{\mathrm{res}} / \rho_{\mathrm{BM}}$, where the bulk density of biomass $\rho_{\mathrm{BM}} \sim 100$ kg m^{-3}. Figure 3(b) plots the characteristic dimension $L_r \sim R_r \sim V_r^{-1/3}$, for the different reaction steps. We can see that a realistic dimension on the order of one or several meters can be achieved when the biomass solid devolatilization is carried out at the higher temperatures (above 250°C). At a lower temperature, torrefaction reaction proceeds very slowly, and the required solid residence time is long, such that the required reactor dimension is prohibitively large. Therefore, in

our reactor design, a higher-temperature, shorter-residence-time treatment is preferred over a lower-temperature, longer-residence-time one. This is consistent with the observations by Prins [17]. Continuing the analysis above, by assuming a characteristic reactor dimension of 1 m, and a maximum residence time of 10^4 s, we found the characteristic velocity of the biomass through the reactor is $v_s \sim 10^{-4}$ m s^{-1}. This implies that the characteristic mass flux of the biomass through the reactor is $\Phi_s \sim \rho_{BM} v_s \sim 0.01$ kg m^{-2} s^{-1}.

One major caveat is that the model above was proposed by fitting experimental data in an idealized reactor set-up in inert conditions. The chemical kinetics could be very different in the oxygen-lean torrefaction regime. However, to our knowledge there is currently no detailed chemical kinetics study carried out under such regime, and it is outside the scope of this work to quantify the chemical kinetics in detail. Therefore, for the purpose of general reactor sizing, we chose to utilize the Bates and Ghoniem mechanism as the best alternative substitution.

3.2 Particle-Scale Effects

Depending on the thermal thickness of the biomass particles, the timescale for heat to penetrate into the biomass particle could also be significant, leading to thermal gradient over the particle and inhomogeneous torrefaction. This problem has been observed previously in torrefaction reactor designs such as fluidized bed [18] and microwave [19]. To understand whether or not this particle-scale effect could cause problems for our reactor concept, we select three diverse types of commonly available biomass in our

vicinity to analyze and later experimentally test: pine shavings, hay, and rice husks. All these biomass types are also fairly common or resemble common crop and forest residues in India, our case study country. As shown in Table S2 in the Supplementary Section, these types of biomass generally have equivalent spherical diameters of less than 10 mm. The particle-scale effects in the torrefaction regime have been considered earlier by Bates and Ghoniem [18]. This study showed that, as long as the particle thickness is less than ~10 mm, the overall heating timescale is slow compared to intraparticle effects. If processing of larger biomass particles is desired, then either such particles need to be first reduced in size, or the reactor configuration (which, as will be explained below, affects the heat transfer timescale) will need to be adjusted accordingly.

3.3 Reactor-Scale Heat Transfer Description

3.3.1 Mechanisms of Heat Transfer

How do we describe the heat transfer characteristics within the biomass moving bed? To inform the modeling process, we examined the literature for modeling counterflow moving bed biomass gasifiers (downward-moving biomass and upward-moving gas). Even though the fundamental thermochemistry of gasification and torrefaction is different, we assume that the physical heat transfer properties through the moving bed should be similar.

We first note that the moving bed itself actually consists of two inhomogeneous phases: a solid phase (biomass) and a gas phase (a mixture of air, volatile gases, and post-combustion

221 flue gases). The two phases transfer heat differently in the axial direction, and the two
222 phases can also exchange heat with each other. We will analyze each phase separately.
223
224 *Solid-phase conduction and radiation.* The actual heat transfer coefficient k_s in the solid
225 phase is a complex interplay of (i) heat conduction within a single biomass particle, (ii)
226 biomass particle-to-particle contact conduction, (iii) particle-to-particle radiation via the
227 porous void, and so forth. In simplifying these effects, we searched for the closest possible
228 lump-sum description in the moving-bed biomass gasifier literature, and utilized the
229 empirical correlations given by Hobbs [20]. In the thermochemical regime of interest, $k_s \sim$
230 1 W m^{-1} K^{-1}. Working from this value, the characteristic heat transfer timescale due to solid-
231 phase conduction and radiation can be approximated as [18] $\rho_s c_{ps} L_r^2 / k_s \sim 10^5$ s, where $L_r \sim$
232 1 m is the axial length of the reactor, $\rho_s \sim 100$ kg m^{-3} the bulk solid density in the moving
233 bed, and $c_{ps} \sim$ 1,000 J kg^{-1} K^{-1} the specific heat capacity of the gas phase.
234
235 *Gas-phase conduction, natural convection, and radiation.* We first consider conduction,
236 natural convection and radiation in the gas phase (independently from the axial advective
237 effects). Similar to the solid effective bulk thermal conductivity k_s, the combined effects of
238 conduction, convection, and radiation in the gas phase can be described by an effective bulk
239 thermal conductivity k_g inside the biomass moving bed, with the empirical correlations
240 given in Hobbs [20]. In our regime of interest, $k_g \sim 0.01$ W m^{-1} K^{-1}. The characteristic heat
241 transfer timescale due to gas-phase conduction, convection, and radiation can be
242 approximated as $\rho_g c_{pg} L_r^2 / k_g \sim 10^5$ s, where $\rho_g \sim 1$ kg m^{-3} the gas density in the moving bed,
243 and $c_{pg} \sim$ 1,000 J kg^{-1} K^{-1} the specific heat capacity of the solid phase.

Axial advection: Both the solid and gas phases are continuously moving axially (in counterflow) inside the reactor, and therefore they carry enthalpies with them. In the solid phase, we have already determined above that, in order to satisfy the residence time requirement, its downward velocity in the reactor, its superficial flow velocity v_s is on the order of 10^{-4} m s^{-1}. Therefore, its characteristic advective timescale within the reactor (of dimension 1 m) is on the order of 10^4 s. To determine the characteristic advective timescale of the gas phase, we note that the stoichiometric air-biomass ratio for complete combustion of biomass is typically in the range of 4-7 on a mass basis [21]. From this, we estimate that in the oxygen-lean combustion regime, the amount of air flux to supply into the reactor is likely on the same order as the amount of biomass flux (or an effective excess air ratio of ~0.2):

$$\Phi_{\mathrm{air}} \sim \Phi_{\mathrm{BM}} \sim 0.01 \text{ kg m}^{-2} \text{ s}^{-1}.$$

Therefore, the gas-phase characteristic advective timescale is on the order of $L_r \rho_g / \Phi_{\mathrm{air}}$ ~100 s, and its characteristic velocity, $v_g \sim \Phi_{\mathrm{air}} / \rho_g \sim 0.01$ m s^{-1}, which is about 100 times faster than the solid-phase movement.

Solid-gas heat transfer. In the biomass moving bed, the solid and the surrounding gas can exist at different temperatures (T_s and T_g, respectively), and there may be heat transfer between the two phases governed by the lump-sum heat transfer coefficient h_{sg}. According to prior studies [22-27], for biomass moving bed, $h_{sg} \sim 10$ W m^{-2} K^{-1}. It can be shown that the timescale of the solid-gas heat transfer can be approximated by $\rho_s c_{p,s} d_p / h_{sg}$ ~100 s, assuming that $d_p \sim 0.01$ m from Table S2.

Heat losses: Both the solid and gas phases can interact with the insulated reactor wall and transfer heat through the wall to the ambient (with a lower temperature T_{amb}). The heat transfer from the moving bed (gas and solid phases) to the reactor side wall is the first step of the heat loss, and this is characterized by two heat transfer coefficients defined in [28-30], the gas-to-wall heat transfer coefficient $h_{\text{gw}} \sim 1$ W m^{-2} K^{-1}, and the solid-to-wall heat transfer coefficient $h_{\text{sw}} \sim 0.01$ W m^{-2} K^{-1}. Therefore, the timescale of gas-to-wall heat transfer is given by $\rho_g c_{p,g} R_r / h_{\text{gw}}$ which depends on the reactor diameter. For a small laboratory-scale equipment, $R_r \sim 0.05$ m which means that the gas-to-wall timescale is on the order of 100 s, but as we scale up the reactor for commercial deployment at $R_r \sim 1$ m, the timescale is lengthened to 1,000 s. On the other hand, for the solid-to-wall heat transfer, the timescale, expressed by the term $\rho_s c_{ps} R_r / h_{\text{sw}}$, is 10^7 s at $R_r \sim 0.05$ m, and 10^8 s at $R_r \sim 1$ m.

3.3.2 Analysis of Heat Transfer Timescales

Having described the various types of heat transfer mechanisms above, we are now poised to answer the following questions: Which of these is the rate-limiting step in the heat transfer process? Which steps of heat transfer occur so rapidly that we can approximate them as almost instantaneous? Figure 3 summarizes the different heat transfer timescales calculated in the previous section.

We can see that, in the regime of the torrefaction reactor dimensions (height ~ 40 cm), heat transfer through advection (both solid and gas phases) occurs much more rapidly than

bulk effective conduction in the respective phases. Therefore, axially, heat transfer is carried out primarily by the gas-phase advective pathway. Furthermore, gas advection occurs on a timescale 100 times faster than solid advection, suggesting that the solid phase migrates downward so slowly that, in the timescale of the upward gas migration, the solid phase may be treated as pseudo-static. However, as the heat exchange between the solid and gas phases also occur quickly, this suggests that as soon as the heat is carried up axially in the gas phase, the surrounding solid is rapidly heated up without advecting too much of this heat back down towards the bottom of the reactor. While it is tempting to state that, due to the high rate of thermal exchange between the solid and gas phases, $T_g \approx T_s$, prior studies have shown that this approximation is not always valid in moving bed biomass gasifiers [31-32]. Finally, at the laboratory scale ($R_r \sim 0.05$ m), the rate of heat loss from the reactor in the gas phase occurs comparatively rapidly with respect to the residence time (advection timescale). Therefore, heat losses to the reactor wall also cannot be ignored when the test reactor is small. This perspective is contrary to many recent approaches to modeling biomass gasifier, which sometimes ignore heat losses from the side wall [33]. As the reactor is scaled up, we expect the magnitude of the heat loss rate to be reduced inversely to the reactor diameter.

In Part II of the study, a more detailed mathematical modeling based on the above-mentioned analysis will shed further light into the actual dimensions of the reaction zone, the relative magnitudes of the various heat transfer pathways, as well as how these quantities change as the reactor is scaled up. For now, from the above-mentioned analysis, we will size and design a preliminary experimental reactor and operate it at about $\Phi_{BM} \sim$

312 $\Phi_{air} \sim 0.01$ kg m^{-2} s^{-1} (calculated from Figure 3 above) to show that the reactor can indeed
313 support biomass torrefaction.

314 **4. Experimental Set-Up and Design**

315 In the previous section, we have gained a coarse-grained understanding of the significant
316 chemical and thermal processes occurring within the reactor. In this section, we describe
317 how we designed and built an experimental apparatus to test our design concept further.
318
319 In order to control the torrefaction conditions under the proposed direct oxygen lean
320 conditions, the test reactor needs to be able to control two independent variables that
321 dominate the chemistry of torrefaction: the solid-phase residence time, and the reactor
322 temperature, which itself depends on how much air is injected relative to how much
323 biomass passes through the reactor. In the next section, we describe our strategies for
324 controlling these two independent parameters.

325 *4.1 Control of Solid Residence Time*

326 A lab-scale, continuous-flow biomass torrefaction reactor design for a feedstock capacity of
327 about 1 kg/h and a cross-sectional diameter of 10.2 cm, was fabricated and tested in this
328 study. This test reactor utilizes a moving-bed reactor concept (labeled in Figure 4a), with
329 an auger at the bottom with the function of continuously removing the torrefied biomass.
330 The auger was sized to be 61 cm (2 feet) in length in order to allow sufficient time for the
331 hot, torrefied biomass to cool off before it exits the reactor outlet. The auger is connected to

a motor drive with an adjustable speed, so that we are able to control the solid-phase residence time inside the reactor for the torrefaction reaction.

In order to calculate the solid residence time, the density ρ_{BM} and input mass flow rate $\dot{m}_{BM}$ of biomass were measured for each type of biomass and auger rotational speed. Given the radius R_r and height H_r of the fixed-bed reactor, the effective residence time τ_{res} of biomass is obtained from:

$$\tau_{\mathrm{res}} = \frac{\rho_{\mathrm{BM}} \pi R_r^2 H_r}{\dot{m}_{\mathrm{BM}}}.$$

Given our specific lab-scale reactor dimensions (diameter = 10.2 cm, depth of torrefaction zone ~ 10 cm), in Table 2, we provide the typical range of possible input feed rates corresponding to the normal ranges of torrefaction residence times.

It can be seen that for our lab-scale reactor, by fixing the torrefaction residence time, the biomass feeding rate is generally on the order of 0.1-2 kg/h. While this is sufficient for lab-scale tests for biomass samples in small quantities, at scale, a commercial torrefaction reactor capable of processing about 500 kg/h of biomass will need to be increased by a factor of 250-5,000. In terms of the reactor diameter, this will be an increase of a factor of 16-71. These numbers are, once again, consistent with the analysis above in Figure 3.

4.2 Control of Torrefaction Severity

At a given solid residence time (i.e. feed rate and reactor volume), in order to control the torrefaction severity, we need to introduce air in different proportions to the solid feedrate.

As shown in Figure 4(c), in order to achieve this, we introduced two air flow inlets near the base of the fixed bed reactor. These inlets are connected to a compressed air cylinder (Airgas AI D300). A mass flow controller (Omega Engineering FMA-5528A) was used to adjust the input air flow rate, with an adjustable flow rate range between 0.1 to 50.0 standard L/min. We divide the mass flow rate of air by the mass flow rate of the incoming biomass to obtain a dimensionless air-biomass ratio (ABR). For normal operations, with an ABR ~ 1.0, the typical air flow rate is set to ~10 L/min, depending on the specific type of biomass and its specific solid mass flow rate.

5. Demonstration of Stable Operating Conditions

Once we have defined the independent parameters (solid residence time τ_{res} and the air-biomass ratio), we can select a few combinations of (τ_{res}, ABR) to demonstrate that the torrefaction reactor can indeed operate continuously and stably.

In order to monitor the reactor operation, we inserted 10 thermocouples, in approximately 2.5-cm spacing, axially throughout the length of the reactor (Figure 5a). As a sample proof of steady-state operation, we flowed air into the reactor at the normalized air-biomass ratio of ABR = 1.0, and the screw auger turning rate was adjusted such as the solid residence time τ_{res} = 11 min. We then ignited some initial pine shavings at the bottom of the reactor, and continuously fed pine shavings from the top such that the level of pine shavings at the top was maintained constant. After an initial start-up period, where the entire reactor assembly and the fixed bed were heated up, a steady-state condition was reached at each axial location, and we demonstrated that the steady-state condition could

be sustained for at least 100 minutes before turning the reactor off by quenching the torrefaction reaction with inert nitrogen in place of air. The mean steady-state temperature readouts at different axial locations were compiled into an axial temperature profile of the reactor (Figure 5b). We note that the fixed bed temperature increases axially towards the bottom of the reactor, and reaches a maximum near where the air inlets are located. The maximum temperature measured, reaching above 200°C, is within the torrefaction regime.

We have demonstrated a stable reactor steady state for one particular reactor operating condition for pine shavings. In order to show that this is not a one-off coincidence, the next question that we address is: Can we show steady states for a wide range of reactor conditions? We operated the reactor under additional conditions, by first changing the air-biomass ratio (τ_{res} = 11 min, ABR = 2.0), then changing the residence time also (τ_{res} = 37 min, ABR = 2.4), and finally changing the biomass type from pine shavings to rice husks. Figure 6a-d show that each of these conditions also result in stable steady-state temperature profiles. Notably, in (b), compared to (a) as we increase the torrefaction severity by introducing more air, we observe a higher measured temperature, as expected. In (c), compared to (a), we observe a gentler increase in the measured temperature profile throughout a broader region of the reactor, because as we increase the solid residence time given the same reactor dimension, we are also reducing the downward solid flux. Therefore, the upward countercurrent gas flux will carry the heat from the bottom of the reactor further up. In (d) compared to (a), we observe a sharper increase in the measured temperature profile as we switch from pine shavings to rice husks, because rice husks have

a higher bulk bed density, which means a reduced effective axial effective thermal conductivity.

To further demonstrate that the reactor outputs are indeed torrefied biomass instead of just burned ash, we subject the output from each of the experiments to proximate analysis (TA Instruments Q50 TGA using the ASTM D-3175 standard), ultimate (elemental) analysis (Thermo Finnigan Flash EA 1112 CHON Analyzer using the ASTM-D5373-16 standard), and bomb calorimetry (Parr Instrument Model 6200 isoperibol). These results are detailed in Table 4, in comparison with the same analysis for raw (untreated) biomass in Table 3.

In interpreting the various results given in Table 4, we also obtained the proximate analysis, ultimate analysis, and bomb calorimetry measurements for raw pine shavings and raw rice husks (presented in Table 3). Firstly, in terms of the higher heating value (HHV), that of raw pine shavings is around 20.5 ± 1.0 MJ kg^{-1}, and that of rice husks is around 15.8 ± 1.0 MJ kg^{-1}, on a dry basis. Therefore, all the experiments above have raised the HHV values of the raw biomass by different amounts. This is consistent with the energy densification effect of biomass torrefaction. Secondly, in terms of the fixed carbon, that of raw pine shavings is 8% ± 1% and that of rice husks, 12% ± 2%, on a dry basis. In comparison, we also see elevated fixed carbon readouts in all the outputs from the different experiments, consistent with biomass torrefaction. Finally, we note that for raw pine shavings, the elemental composition is such that (C, H, O) = (49.6%, 5.7%, 44.8%), and for raw rice husks, (C, H, O) = (37.6%, 3.9%, 58.3%), on a dry basis. By comparing these baseline values with those obtained in the experimental outputs, we observe that our

reactor conditions cause the raw biomass to gain carbon and lose oxygen. These chemical changes are also consistent with biomass torrefaction. As we make the torrefaction conditions more severe such as by increasing the air-biomass ratio, we notice that HHV, fixed carbon content, elemental carbon content are also increased, while elemental hydrogen and oxygen contents are decreased. These are consistent with the expected principles and trends of biomass torrefaction, which increases the energy content and carbon content in the raw biomass. Another interesting point to note is that, as ash does not volatilize in biomass torrefaction, any torrefaction reaction tends to concentrate the amount of ash in the torrefied biomass. This is especially remarkable in the case of rice husks, which already have a high ash content to start with, and in our torrefied rice husk sample, more than a third of the mass constitutes ash. We expect that the presence of this inert solid will make our torrefaction reactor operation less efficient with respect to high-ash biomass feedstock varieties.

There is much more that can be quantified regarding the reactor operations, and the scope of this present paper is to demonstrate the initial validation data for our experimental set-up. In a subsequent study, we will develop a fine-grained model description of these experimental data in order to better understand the scaling law of this reactor concept. We will also define more concrete performance metrics, and conduct a more systematic mapping of the reactor conditions to these performance metrics under a wider range of biomass.

6. Conclusion and Discussions

6.1 Conclusion

In Part I of this two-part study, we presented a case for the design and development of a small- to medium-scale torrefaction reactor for decentralized deployment in rural areas. Based on the concept of oxygen-lean torrefaction, we developed a countercurrent moving bed reactor. By performing a multi-scale analysis and subsequently implementing a laboratory-scale reactor set-up, we showed that the temperature profiles, output solid higher-heating value, proximate analysis, and elemental analysis values are generally consistent with generally accepted biomass torrefaction conditions. This validates our reactor concept, and shows that it can indeed satisfy the requirements for biomass torrefaction.

6.2 Discussion

In Part II of the study, we will develop a more detailed mathematical model description, based on the multi-scale analysis performed above. In subsequent studies, we will also introduce a framework where we can systematically map various performance metrics of this oxygen-lean torrefaction reactor. Of course, the validation of our oxygen-lean torrefaction reactor concept will not be complete until we compare its performance metrics with current torrefaction reactors that operate under inert conditions. This quantitative comparison will also be performed as a part of a future study.

Acknowledgements

The materials and equipment of work were funded by the MIT Tata Center. In addition, KSK would like to acknowledge the MIT Tata Center Fellowship, the Dolores Zohrab Liebmann Fellowship, as well as the Legatum Fellowship for supporting his tuition and stipend as a doctoral student. The authors declare no competing interest.

Bibliography

[1] B. Acharya, A. Dutta, Fuel property enhancement of lignocellulosic and nonlignocellulosic biomass through torrefaction, *Biomass Conversion and Biorefinery* 6 (2015) 139-149.

[2] J.S. Tumuluru, S. Sokhansanj, J.R. Hess, C.T. Wright, and R.D. Boardman, A review on biomass torrefaction process and produt properties for energy applications, *Industrial Biotechnology* 7 (2011) 384-401.

[3] B. Arias, C. Pevida, J. Fermoso, M.G. Plaza, F. Rubiera, J.J. Pis, Influence of torrefaction on the grindability and reactivity of woody biomass, *Fuel Processing Technology* 89 (2008) 169-175.

[4] D. Thrän, J. Witt, K. Schaubach, J. Kiel, M. Carbo, J. Maier, C. Ndibe, J. Koppejan, E. Alakangas, S. Majer, F. Schipfer, Moving torrefaction towards market introduction – Technical improvements and economic-environmental assessment along the overall torrefaction supply chain through the SECTOR project, *Biomass and Bioenergy* 89 (2016) 184-200.

[5] J. Koppejan, Status overview of torrefaction technologies. IEA Bioenergy Task 32 report, 2012.

[6] Kung's book chapter on green charcoal production

[7] S.K. Lowder, J. Skoet, T. Raney, The number, size, and distribution of farms, smallholder farms, and family farms worldwide, *World Development* 87 (2016) 16-29.

[8] M. Laurin, A. Chamberland, Gasification of agricultural residues for energy production, *Energy Sources* 5(4) (1981) 361-80.

[9] K.S. Kung, Design and validation of a decentralized biomass torrefaction system, PhD thesis, Massachusetts Institute of Technology, 2017.

[10] M. Svanberg, I. Olofsson, J. Floden, A. Nordin, Analysing biomass torrefaction supply chain costs, *Bioresource Technology* 142 (2013) 287-96.

[11] C. Wang, J. Peng, H. Li, X.T. Bi, R. Legros, C.J. Lim, S. Sokjansanj, Oxidative torrefaction of biomass residues and densification of torrefied sawdust to pellets, *Bioresource Technology* 127 (2013) 318-25.

[12] K.M. Lu, W.J. Lee, W.H. Chen, S.H. Liu, T.C. Lin, Torrefaction and low temperature carbonization of oil palm fiber and eucalyptus under nitrogen and air atmospheres, *Bioresource Technology* 123 (2010) 98-105.

[13] W.H. Chen, K.M. Lu, S.H. Liu, C.M. Tsai, W.J. Lee, T.C. Lin, Biomass torrefaction characteristics in inert and oxidative atmospheres at various superficial velocities, *Bioresource Technology* 146 (2013) 152-60.

[14] W.H. Chen, K.M. Lu, W.J. Lee, S.H. Liu, T.C. Lin, Non-oxidative and oxidative torrefaction characterization and SEM observation of fibrous and ligneous biomass, *Applied Energy* 114 (2014) 104-13.

[15] R. Bates, A.F. Ghoniem, Biomass torrefaction: Modeling of volatile and solid product evolution kinetics, *Bioresource Technology* 124 (2012) 460-9.

[16] B. Peters, C. Bruch, Drying and pyrolysis of wood particles: experiments and simulation, *J. Analy. Appl. Pyrolysis* 70 (2003) 233-50.

[17] M.J. Prins, Thermodynamic analysis of biomass gasification and torrefaction, PhD thesis, Eindhoven University of Technology, 2005.

[18] R. Bates, A.F. Ghoniem, Modeling kinetics-transport interactions during biomass torrefaction: The effects of temperature, particle size, and moisture content, *Fuel* 137 (2014): 216-29.

[19] A. Dhungana, P. Basu, A. Dutta, Effects of reactor design on the torrefaction of biomass, *Journal of Energy Resources Technology* 134 (2012).

[20] M.L. Hobbs, P.T. Radulovic, L.D. Smoot, Modeling fixed-bed coal gasifiers, *AIChE* 38(5) (1992) 681-702.

[21] B.M. Jenkins, L.L. Baxter, T.R. Miles Jr., T.R. Miles, Combustion properties of biomass, *Fuel Processing Technology* 54 (1998) 17-46.

[22] T.H. Chilton, A.P. Colburn AP, *Ind. Eng. Chem.* 26 (1934) 1183.

[23] B.W. Gamson, G. Thodos, O.A. Hougen, *Trans. Am. Inst. Chem. Engrs.* 39 (1943) 1.

[24] J. De Acetis J, G. Thodos, *Ind. Eng. Chem.* 52 (1960) 1003.

[25] A.S. Gupta, G. Thodos, Direct analogy between mass and heat transfer to beds of spheres, *AIChE* 9(6) (1963) 751.

[26] C. Di Blasi C, Modeling wood gasification in a countercurrent fixed-bed reactor, *AIChE* 50(9) (2004) 2306-19.

[27] P.T. Radulovic, M.U. Ghani, L.D. Smoot, An improved model for fixed bed coal combustion and gasification, *Fuel* 74(4) (1995) 582-94.

[28] C. Di Blasi C, Dynamic behavior of stratified downdraft gasifiers. *Chemical Engineering Science* 55 (2000) 2931-44.

[29] G.F. Froment, K.B. Bischoff, *Chemical Reactor Design.* Wily, New York, 1979.

[30] A.P. DeWasch, G.F. Froment GF, A two-dimensional heterogeneous model for fixed bed catalytic reactors, *Chem Eng Sci* 26 (1971) 629.

[31] J. Cooper, W.L.H. Hallett, A numerical model for packed-bed combustion of char, *Chemical Engineering Science* 55 (2000) 4451-60.

[32] L. Rosa, R. Tosat, Modelling and testing a cogeneration plant based on wood gasification, 7th European Conference on Industrial Furnaces and Boilers, 2006.

[33] M. Puig-Arnavat, J.C. Bruno, A. Cornoas, Review and analysis of biomass gasification models, *Renewable and Sustainable Energy Review* 14 (2010) 2841-2851.

FIGURES

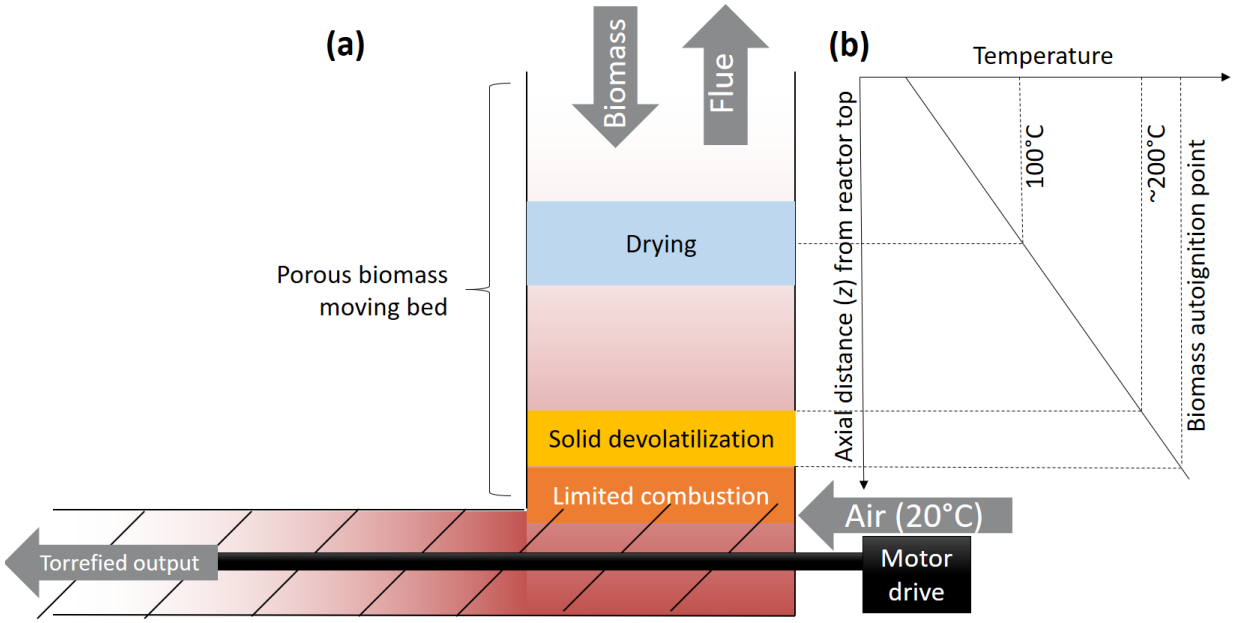

Figure 1 – (a) Schematic of an oxygen-lean moving bed torrefaction reactor design. (b) Guessed axial temperature profile along the reactor.

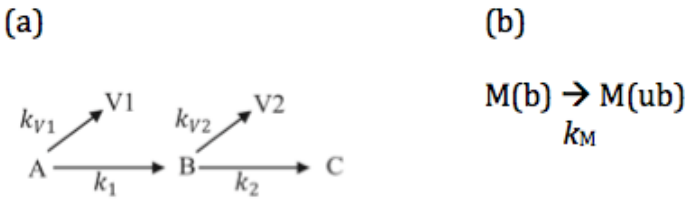

Figure 2 - A simplified kinetics model for torrefaction and drying. (a) A kinetic description of the solid devolatilization kinetics during biomass torrefaction, as proposed by Bates and Ghoniem [10]. (b) A one-step simplified model describing drying kinetics in biomass, as adopted from Peters and Bruch [11].

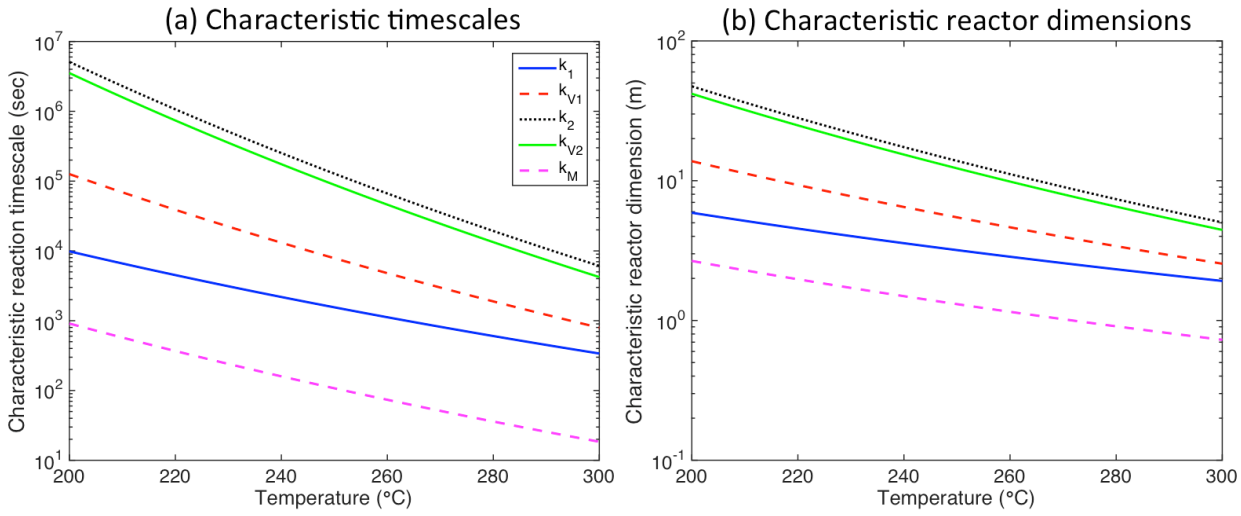

589

590 Figure 3. (a) Characteristic timescales and (b) characteristic reactor dimensions related to

591 the various solid devolatilization and drying steps in biomass torrefaction.

592

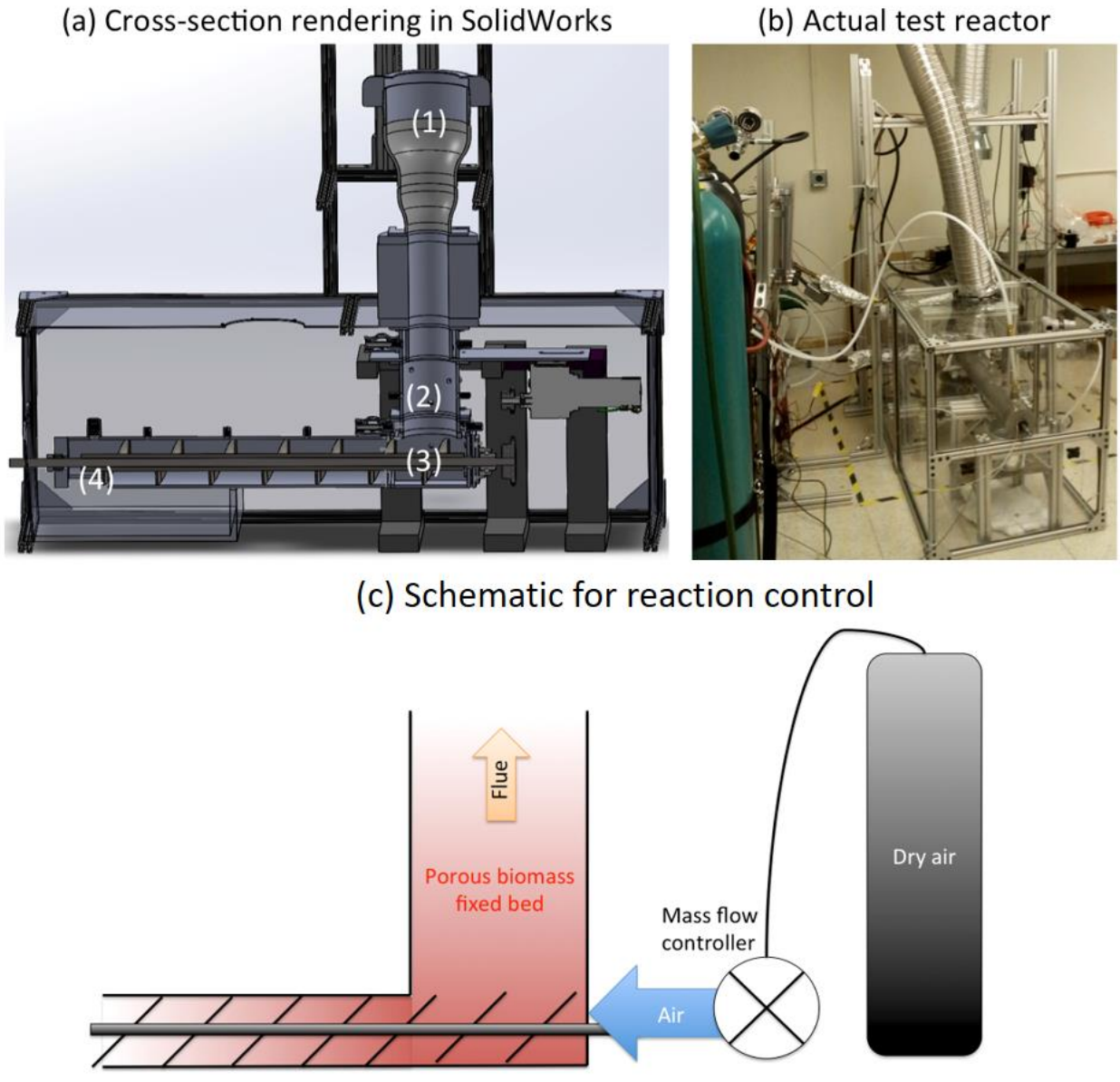

593

594 Figure 4 - A lab-scale biomass torrefaction reactor was designed and built. (a) Cross-
595 section rendering of the reactor design in SolidWorks, with biomass feeding inlet (1), fixed-
596 bed reactor zone (2), screw auger (3), and torrefied product outlet (4) labeled. (b) An
597 actual lab-scale test reactor assembly in operation. (c) We utilized adjustable air flow inlets
598 to control torrefaction severity. As shown in the schematic, the air is injected at the bottom
599 of the reactor and its flow rate is controlled via a mass flow controller.

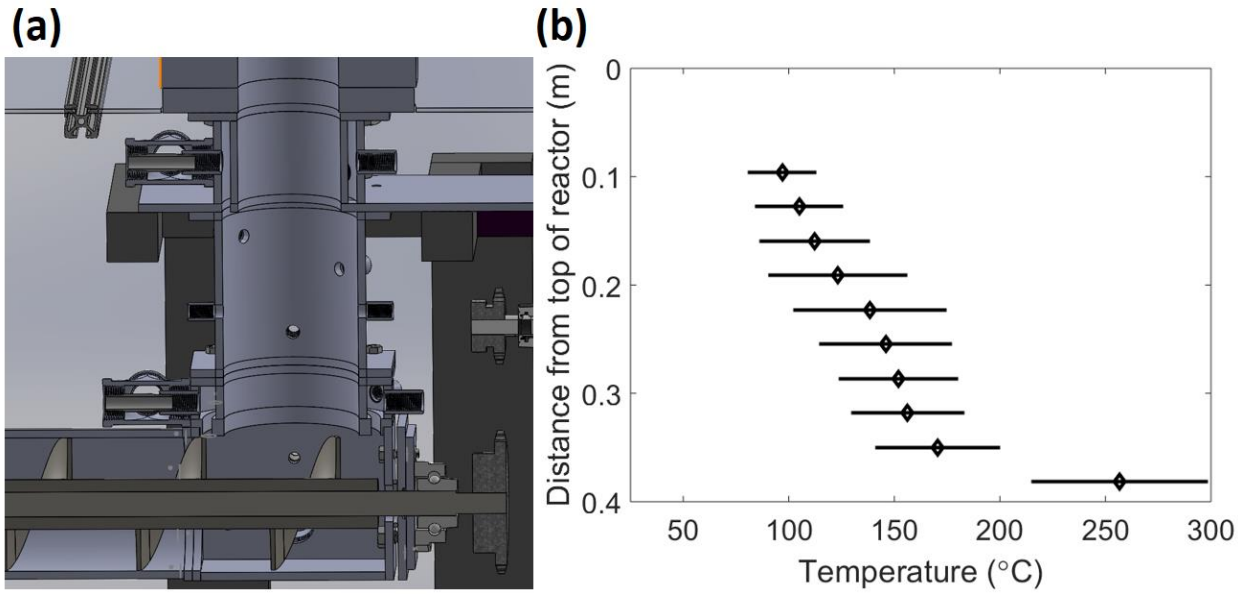

Figure 5 - Sample steady-state temperature validation for the torrefaction reactor operating on pine shavings, with the following reaction conditions τ_{res} = 11 min, ABR = 1.0. (a) Throughout the axial length of the reactor, various thermocouples are placed about 2.5 cm apart to measure the temperature at each point in the biomass fixed bed. This schematic is juxtaposed next to the distance axis in (b) to illustrate the locations of each temperature measurement at the center of the moving bed reactor in the context of the larger reactor design. (b) A stable steady-state axial temperature profile consistent with torrefaction conditions, with error bars indicated, is achieved for at least 100 minutes.

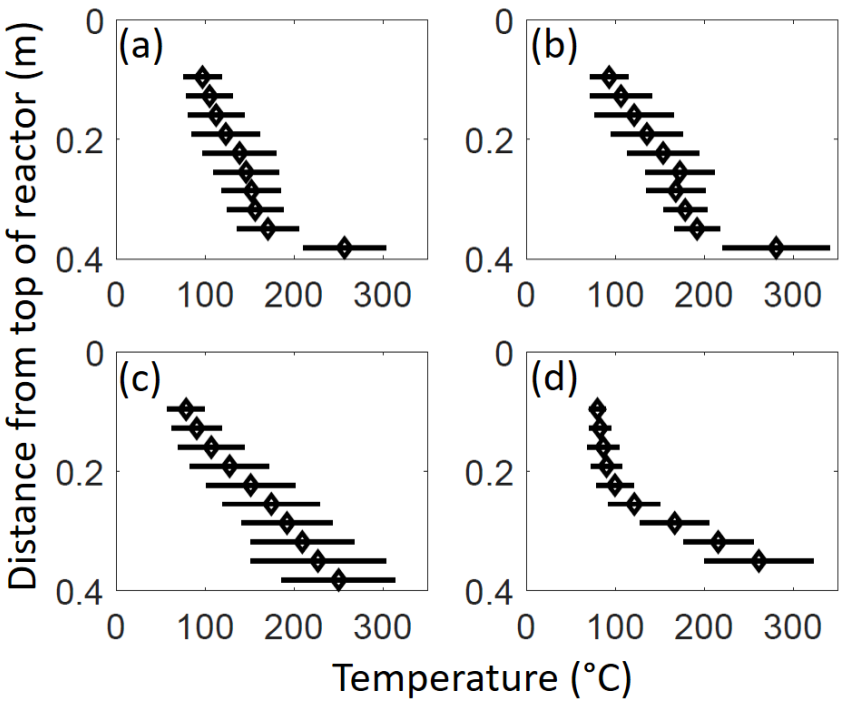

610

611 Figure 6 - Steady-state temperature profiles were achieved under a variety of reactor
612 operating conditions, for pine shavings for the torrefaction reactor under various operating
613 conditions: (a) τ_{res} = 11 min, ABR = 1.0, and (b) τ_{res} = 11 min, ABR = 2.0, and (c) τ_{res} = 37
614 min, ABR = 2.4. We also operated the reactor using (d) rice husks, with τ_{res} = 27 min, ABR =
615 1.0.

616

TABLES

Table 1 – Characteristic timescales of the various heat-transfer mechanisms, with a lab-scale reactor R_r = 0.05 m.

Heat transfer mechanism	Characteristic timescale
Solid-phase bulk effective conduction	$\frac{\rho_s c_{ps} L_r^2}{k_s} \sim 10^5$ s
Gas-phase bulk effective conduction	$\frac{\rho_g c_{p,g} L_r^2}{k_g} \sim 10^5$s
Gas-phase advection	$\frac{L_r}{v_g} \sim 10^2$s
Solid-phase advection	$\frac{L_r}{v_s} \sim 10^4$s
Gas-to-wall heat loss	$\frac{\rho_g c_{p,g} R_r}{2h_{\mathrm{gw}}} \sim 10^2 - 10^3$ s
Solid-to-wall heat loss	$\frac{\rho_s c_{p,s} R_r}{2h_{\mathrm{sw}}} \sim 10^7 - 10^8$ s
Solid-gas exchange	$\frac{\rho_s c_{p,s} d_p}{h_{sg}} \sim 10^2$ s

623 Table 2 - Typical ranges of possible input feeding rates in our lab-scale reactor for different
624 solid residence times. The possible ranges of feeding rates depend significantly on the type
625 of biomass.

Residence time	5 min	20 min	40 min
Pine shavings / hay	0.58 kg/h	0.15 kg/h	0.073 kg/h
Rice husk	2.0 kg/h	0.51 kg/h	0.26 kg/h

626

627 Table 3 - Proximate analysis, ultimate (elemental) analysis, and higher heating value
628 measured on the raw (untreated) pine shavings and rice husks used for our experiments,
629 on a dry basis. The error bars are based on triplicate measurements.

Biomass type	Pine shavings	Rice husks
Bulk density	30 kg m^{-3}	100 kg m^{-3}
HHV (dry basis)	20.5 ± 1.0 MJ kg^{-1}	15.8 ± 1.0 MJ kg^{-1}
Fixed carbon	8 ± 1%	12 ± 2%
Ash content	1.6 ± 1%	17.0 ± 2%
Elemental C	49.6%	37.6%
Elemental H	5.7%	3.9%
Elemental O	44.8%	58.3%

630

631 Table 4 – Proximate analysis, ultimate (elemental) analysis, higher heating value, and yield
632 values measured on the solid fuel outputs from the different experiments, on a dry basis.

Parameter	Experiment (a)	Experiment (b)	Experiment (c)	Experiment (d)
Biomass type	Pine shavings	Pine shavings	Pine shavings	Rice husks
Residence time	11 min	11 min	37 min	27 min
ABR	1.0	2.0	2.4	1.0
Output HHV	25.1 MJ kg^{-1}	27.3 MJ kg^{-1}	23.8 MJ kg^{-1}	17.6 MJ kg^{-1}
Fixed carbon	31%	41%	32%	48%
Ash	0.8%	0.9%	1.0%	37%
Elemental C	58%	66%	61%	44%
Elemental H	5%	4%	5%	2%
Elemental O	37%	30%	35%	54%
Mass yield	51%	36%	52%	62%
Energy yield	63%	47%	60%	69%

633
634

SUPPLEMENTAL MATAERIALS

Supplemental Table S1 – Design production capacities of different torrefaction technologies [1]

Torrefaction Technology	Design	Production Capacity
Torr-Coal (the Netherlands)	Rotary drum	110 tons day^{-1}
BioEndev (Sweden)	Screw conveyor	50 tons day^{-1}
Solvay (USA)	Screw conveyor	800 tons day^{-1}
Topell (the Netherlands)	Fluidized bed	190 tons day^{-1}
River Basin Energy (USA)	Fluidized bed	140 tons day^{-1}
ECN (NL) / Andritz (Denmark)	Moving bed	20 tons day^{-1}
Thermya/Areva (France)	Moving bed	60 tons day^{-1}

Supplemental Table S2 – Characteristic dimensions of sample biomass particles, as computed by averaging 100 sample biomass particles from each type. The sample photo illustrates how the lengths of major and minor axes are measured.

Biomass type	Pine shavings	Hay	Rice husks
Sample photo	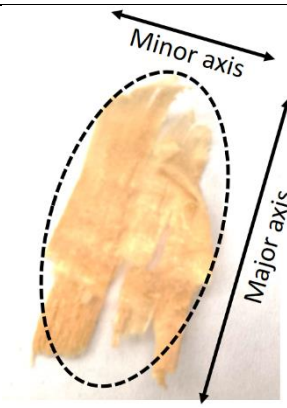		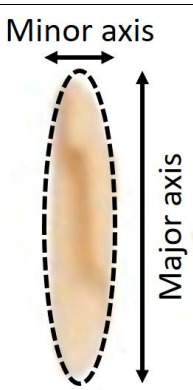
Major axis	11.1 mm	6.4 mm	0.2 mm
Minor axis	6.4 mm	4.4 mm	1.8 mm
d_p	3.0 mm	9.4 mm	2.9 mm